A numerical analysis of the impact of gas pressure and dielectric material on the generation of body force in an air gas plasma actuator

Sajad Hajikhani, Ramin Mehrabifard, Hamed Soltani Ahmadi

▶ **To cite this version:**

Sajad Hajikhani, Ramin Mehrabifard, Hamed Soltani Ahmadi. A numerical analysis of the impact of gas pressure and dielectric material on the generation of body force in an air gas plasma actuator. Radiation Physics and Engineering, 2024, 5 (2), pp.51-60. 10.22034/rpe.2024.429773.1176 . hal-04553553

HAL Id: hal-04553553
https://hal.science/hal-04553553

Submitted on 20 Apr 2024

HAL is a multi-disciplinary open access archive for the deposit and dissemination of scientific research documents, whether they are published or not. The documents may come from teaching and research institutions in France or abroad, or from public or private research centers.

L'archive ouverte pluridisciplinaire **HAL**, est destinée au dépôt et à la diffusion de documents scientifiques de niveau recherche, publiés ou non, émanant des établissements d'enseignement et de recherche français ou étrangers, des laboratoires publics ou privés.

Distributed under a Creative Commons Attribution - NonCommercial - NoDerivatives 4.0 International License

RPE | Radiation Physics & Engineering
A Peer-Reviewed Journal
Published by K.N. Toosi University of Technology
http://rpe.kntu.ac.ir
Research Article

Radiation Physics and Engineering 2024; 5(2):51–60

A numerical analysis of the impact of gas pressure and dielectric material on the generation of body force in an air gas plasma actuator

Sajad Hajikhani[a], Ramin Mehrabifard[b,c,*], Hamed Soltani Ahmadi[a,d]

[a] *Department of Atomic and Molecular Physics, Faculty of Science, University of Mazandaran, Babolsar, Iran*
[b] *Department of Physics and Institute for Plasma Research, Kharazmi University, 49 Dr. Mofatteh Avenue, Tehran, Iran*
[c] *Division of Environmental Physics, Faculty of Mathematics, Physics and Informatics, Comenius University, Mlynsk dolina, 84248 Bratislava, Slovakia*
[d] *Plasma Technology Research Core, Faculty of Science, University of Mazandaran, Babolsar, Iran*

HIGHLIGHTS

- Impact of dielectric materials on plasma characteristics and body force in an SDBD plasma actuator.
- The rate of species generation in the plasma actuator is significantly influenced by the dielectric substance.
- Changing the dielectric material does not make a significant difference in electron temperature.
- Electron density changes in response to the change in the dielectric material.
- Ion density is affected by the dielectric material, with mica having the highest ion density and PTFE having the lowest.

ABSTRACT

Plasma technology has undeniably revolutionized industrial processes in recent decades. Atmospheric pressure plasma (APP) has emerged as a prominent and widely applicable tool in various scientific disciplines. Notably, plasma-assisted flow control has become a subject of intense interest, particularly applying surface dielectric barrier discharge (SDBD) plasma actuators for aerodynamic flow control. In this study, a two-dimensional model of the SDBD plasma actuator is developed using the COMSOL Multiphysics program, incorporating air gas discharge reactions with $N_2/O_2/Ar$ gases in specific ratios (0.78, 0.21, 0.01). The investigation focuses on the impact of dielectric materials (mica, silica glass, quartz, and polytetrafluoroethylene (PTFE)) on plasma characteristics and body force within the plasma actuator under constant input parameters. Moreover, the study explores how variable pressure (760, 660, and 560 torr) in different applications influences plasma properties, ultimately affecting the magnitude of the body force in the plasma actuator. These findings contribute to optimizing plasma technology for flow control applications and enhance industrial efficiency and performance.

KEYWORDS

Dielectric Barrier Discharge
Argon Plasma
Plasma Actuator
Body Force
COMSOL Multiphysics
Gas Discharge

HISTORY

Received: 10 December 2023
Revised: 15 January 2024
Accepted: 11 February 2024
Published: Spring 2024

1 Introduction

Since nonthermal plasma first attracted scientific and technical attention 70 years ago, plasma technology has taken center stage in industrial processes both now and in the future. Over time, plasma technology developed and is today employed in everything from everyday items to cutting-edge applications (Keidar and Beilis, 2013). Various scientific sectors have utilized APP because of its outstanding quality (Mehrabifard et al., 2020; Venezia et al., 2008; Da Ponte et al., 2011; Assadi et al., 2022; Mehrabifard et al., 2017). Over the past few years, plasma-assisted flow control has received much interest (Neretti et al., 2014; Touchard, 2008). Significant interest is in utilizing surface dielectric barrier discharge (SDBD) plasma actuators to control aerodynamic flow. Plasma actuators find utility in the realm of active airfoil leading edge separation control (Neretti et al., 2014), used for high lift (Little et al., 2010), boundary layer flow control (Porter et al., 2007; Szulga et al., 2015), handling dynamic stall in an airfoil (Post and Corke, 2006), bluff body flow control (Do et al., 2007), regulation of airflow (Neretti et al., 2012), lowering noise levels (Thomas et al., 2008), and postponing turbine blade separation (Huang et al., 2006). Many studies have

*Corresponding author: ramin94mehrabifard@gmail.com

https://doi.org/10.22034/rpe.2024.429773.1176

been conducted experimentally and numerically, focusing on optimizing the ionic wind velocity and the volumetric force generation mechanism (Likhanskii et al., 2008; Jayaraman and Shyy, 2008; Mahdavi and Sohbatzadeh, 2019; Moreau, 2007). Moreau et al. reviewed the mechanical and electrical characteristics and their applications in aerodynamic flow control (Benard and Moreau, 2014). Numerous earlier numerical research has utilized two or more straightforward reactions to reduce the computations required (Abdollahzadeh et al., 2012; Boeuf et al., 2007; Likhanskii et al., 2007). Additionally, the plasma component may occasionally be viewed under an electrostatic condition (Abdelraouf et al., 2020; Kazemi et al., 2021; Omidi and Mazaheri, 2020; Tehrani et al., 2022; Yu et al., 2023). In some cases, a specific sort of gas has also been applied to this structure (Mehrabifard, 2023).

This study describes a two-dimensional model of the SDBD plasma actuator. The COMSOL Multiphysics program is used in the development of the model. Air gas discharge reactions with the combination of nitrogen, oxygen, and argon gas with a ratio of 0.78, 0.21, and 0.01, respectively, are considered for this simulation. With constant input parameters, we investigate the effect of dielectric material on the plasma characteristics and body force in the plasma actuator. Besides that, the pressure can be variable in many of the mentioned applications, which can change many parameters of the plasma, which, as a result, changes the magnitude of the body force in the plasma actuator.

2 Model Description

2.1 Governing Equations

In this investigation, the fluid model was employed. The electron density and energy can be calculated by resolving the drift-diffusion formulas. To formulate the governing equations of electric discharge, the drift-diffusion approximation was adopted (Mehrabifard, 2023):

$$\frac{\partial n_e}{t} + \nabla.\vec{\Gamma}_e = R_e - (\vec{u}.\nabla)n_e \tag{1}$$

$$\vec{\Gamma}_e = -(\vec{\mu}_e.\vec{E})n_e - \vec{D}_e.\nabla n_e \tag{2}$$

The electron continuity equation is defined by Eq. (1), where n_e is the electron density, D_e is diffusion coefficient, Γ_e is electron flux, u is average species velocity, and R_e is electron generation rate. Equation (2) represents the electron flow, divided into drift and diffusion. The electron energy density can be calculated using this equation:

$$\begin{aligned} &\frac{\partial n_\varepsilon}{t} + \nabla.\vec{\Gamma}_\varepsilon + \vec{E}.\vec{\Gamma}_\varepsilon = R_\varepsilon - (\vec{u}.\nabla)n_\varepsilon \\ &\vec{\Gamma}_\varepsilon = -(\vec{\mu}_\varepsilon.\vec{E})n_\varepsilon - \vec{D}_\varepsilon.\nabla n_\varepsilon \end{aligned} \tag{3}$$

The value of $\vec{E}.\vec{\Gamma}_\varepsilon$ is the amount of energy that can be extracted from an electron by applying an electric field. The following equation may be used to compute the energy gained by non-elastic collisions, which is denoted by the variable R_ε:

$$R_\varepsilon = S_{en} + \frac{Q + Q_{gen}}{q} \tag{4}$$

S_{en} is the power dissipation, Q_{gen} is the heat source, and q is the electron charge. D_e is electron diffusion coefficient, μ_ε indicates energy mobility, and D_ε is energy distribution coefficient. The link between these parameters is shown in Eq. (5):

$$\begin{aligned} D_\varepsilon &= \mu_\varepsilon T \\ D_e &= \mu_\varepsilon T_e \\ \mu_\varepsilon &= \frac{5}{3}\mu_e \end{aligned} \tag{5}$$

The Townsend coefficients of the electron source, which are determined by the following equation, were used:

$$R_e = \sum_{j=1}^{M} x_j a_j N_n |\Gamma_e| \tag{6}$$

where M is the total number of reactions, x_j the molar fraction of the target species for reaction j, a_j is the Townsend coefficient, and N_n is the total number of neutral particles are present. Considering the number p of non-elastic electron collisions, we will have:

$$R_\varepsilon = \sum_{j=1}^{p} x_j a_j N_n |\Gamma_e| \Delta\varepsilon_j \tag{7}$$

where $\Delta\varepsilon_j$ is the energy dissipation of the j reaction. For non-electron-induced species, the below equation is used for mass fraction calculation:

$$\rho\frac{\partial w_k}{t} + \rho(\vec{u}.\nabla)w_k = \nabla.\vec{j}_k + R_k \tag{8}$$

in which w_k is the ionic density and j_k is the energy flux of the ions. The following equation obtains the electrostatic field:

$$\nabla.(\varepsilon_0\varepsilon_r E) = \rho \tag{9}$$

where ε_0 is the permittivity of vacuum and ε_r is a relative dielectric constant. The following relationships are found regarding the boundary conditions for the electron flux and energy flow:

$$-\hat{n}.\vec{\Gamma}_e = (\frac{1}{2}\upsilon_{eth}n_e) - \sum_p \gamma_p(\vec{\Gamma}_p.\hat{n}) \tag{10}$$

$$-\hat{n}.\vec{\Gamma}_\varepsilon = (\frac{5}{6}\upsilon_{eth}n_e) - \sum_p \varepsilon_p\gamma_p(\vec{\Gamma}_p.\hat{n}) \tag{11}$$

The right-hand side of Eq. (10) displays the electron number caused by the secondary electron and γ represents the secondary electron coefficient. Ions and excited species on the surface of electrodes are neutralized via the surface reaction. Surface interactions on the electrode are indicated by the β_j coefficient, which means the probability of the function of the j species. The definition of flux matching for each heavy species is as follows:

$$n.j_k = M_k R_{surf,k} + M_k c_k \mu_{m,k^z k}(n.E)[(z_k n.E) > 0] \tag{12}$$

in which j_k and $R_{surf,k}$ indicate the diffusive flux vector and the surface reaction rate expression for species k. M_k is mass fraction and c_k is particle mass density.

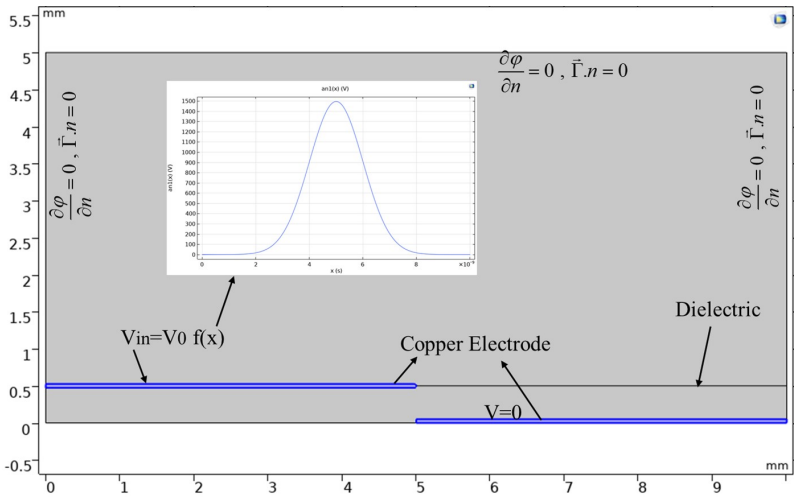

Figure 1: Schematic of the plasma actuator, boundary condition, and input voltage with its function.

The body force generated by plasma is:

$$f_{coulomb} = \rho_\nu \times normE \tag{13}$$

In this equation, ρ_ν is the density of electrons and positive/negative ions, $normE$ is the normalized electric field in the $x - y$ direction. In this simulation, the value of charge density is equal to:

$$\begin{aligned}\rho_\nu =&(n_{Ar^+} + n_{N_{2^+}} + n_{O_{2^+}} + n_{N_{4^+}} + \\ &n_{O_+} + n_{O_{4+}} - n_e - n_{O-})\end{aligned} \tag{14}$$

Table 1: The reactions of electron impact with active species of nitrogen. (Singly ionized nitrogen molecule N_2^+, metastable nitrogen N_2s, nitrogen molecule N_2) (Mehrabifard, 2023; Hagelaar, 2010; LXcat, 2023)

Reactions	Formula	Type	$\Delta\varepsilon$ (eV)
1	e + N_2 → e +N_2	Elastic	0
2	e + N_2 → e +N_2s	Excitation	0.02
3	e + N_2 → e +N_2s	Excitation	0.29
4	e + N_2 → e +N_2s	Excitation	0.291
5	e + N_2 → e +N_2s	Excitation	0.59
6	e + N_2 → e +N_2s	Excitation	0.88
7	e + N_2 → e +N_2s	Excitation	1.17
8	e + N_2 → e +N_2s	Excitation	1.47
9	e + N_2 → e +N_2s	Excitation	1.76
10	e + N_2 → e +N_2s	Excitation	2.06
11	e + N_2 → e +N_2s	Excitation	2.35
12	e + N_2 → e +N_2s	Excitation	6.17
13	e + N_2 → e +N_2s	Excitation	7
14	e + N_2 → e +N_2s	Excitation	7.35
15	e + N_2 → e +N_2s	Excitation	7.36
16	e + N_2 → e +N_2s	Excitation	7.8
17	e + N_2 → e +N_2s	Excitation	8.4
18	e + N_2 → e +N_2s	Excitation	8.16
19	e + N_2 → e +N_2s	Excitation	8.55
20	e + N_2 → e +N_2s	Excitation	8.89
21	e + N_2 → e +N_2s	Excitation	11.03
22	e + N_2 → e +N_2s	Excitation	11.88
23	e + N_2 → e +N_2s	Excitation	12.25
24	e + N_2 → e +N_2s	Excitation	13
25	e + N_2 → 2 e +N_2^+	Ionization	15.6

Table 2: The interactions between oxygen and electrons (Hagelaar, 2010; LXcat, 2023)

Reactions	Formula	Type	$\Delta\varepsilon$ (eV)
1	e + O_2 → e +O_2	Elastic	-
2	e + O_2 → O +O^-s	Attachment	-
3	e + O_2 → e +O_2	Excitation	0.02
4	e + O_2 → e +O_2	Excitation	0.19
5	e + O_2 → e +O_2	Excitation	0.19
6	e + O_2 → e +O_2	Excitation	0.38
7	e + O_2 → e +O_2	Excitation	0.38
8	e + O_2 → e +O_2	Excitation	0.57
9	e + O_2 → e +O_2	Excitation	0.75
10	e + O_2 → e +O_2 a1d	Excitation	0.977
11	e + O_2a1d → e +O_2	Excitation	-0.977
12	e + O_2 → e +O_2b1s	Excitation	1.627
13	e + O_2b1s → e +O_2	Excitation	-1.627
14	e + O_2 → e +$O_2$45	Excitation	4.5
15	e + $O_2$45 → e +O_2	Excitation	-4.5
16	e + O_2 → e +O + O	Dissociation	6
17	e + O_2 → e +O + O1d	Excitation	8.4
18	e + O_2 → e +O1s	Excitation	9.95
19	e + O_2 → 2e +O_2^+	Ionization	12.06

2.2 Boundary Conditions and Reactions

An asymmetric pair of copper electrodes separated by a dielectric substance from the actuator. While the other electrode is connected to the ground and encased by the dielectric material, the first electrode is placed on the dielectric surface and in contact with the gas flow at atmospheric pressure. A Gaussian voltage power supply drives the discharge at 1.5 kV. The electron density is first estimated to be 10^8 m^{-3}. The gas is at a temperature of 293.15 K and a pressure of 760 torr. In the simulation, the material components are defined as a model of the air, considering the related reactions of the species. Rate coefficients were obtained by solving Boltzmann's equation with BOLSIG+ (Hagelaar and Pitchford, 2005) and the cross-sections from the LXCAT data source (Pitchford et al., 2017). Reaction rates were taken from the references (Sakiyama et al., 2012). The dominant reactions can be seen in Tables 1 to 6, including electron impact

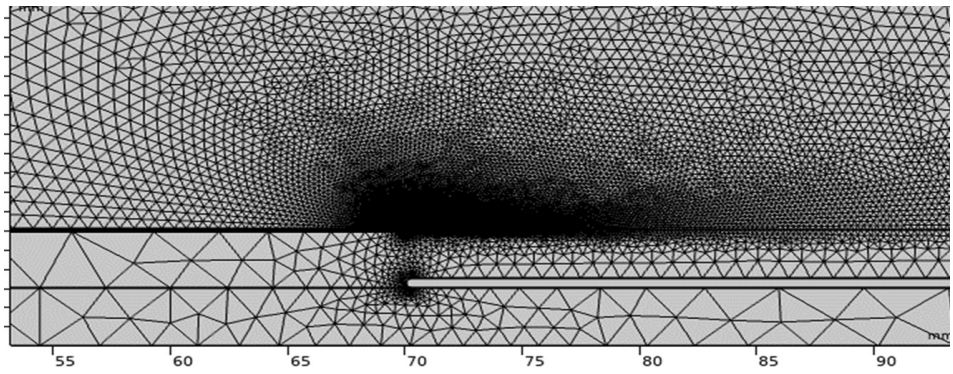

Figure 2: Meshing and its density in edges.

Table 3: Atomic and molecule-to-molecule interactions with two and three bodies (Stafford and Kushner, 2004; Sohbatzadeh and Soltani, 2018).

Reactions	Formula	Type	K^f ($m^3.s^{-1}.mol^{-1}$)
1	$e + N^+ \rightarrow N$	Recombination	3.5×10^{-18}
2	$e + N_2 \rightarrow 2e + N + N^+s$	Dissociative ionization	2.4×10^{-23}
3	$e + N_2 \rightarrow e + 2N$	Dissociative	2×10^{-17}
4	$e + N_2^+ \rightarrow 2N$	-	2.8×10^{-13}
5	$N^+ + N_2 \rightarrow N + N_2^+$	Charge exchange	10^{-17}

Table 4: Atomic and molecule-to-molecule interactions with two and three bodies (Stafford and Kushner, 2004; Sohbatzadeh and Soltani, 2018).

Reactions	Formula	K^f ($m^3.s^{-1}.mol^{-1}$)
1	$O + O_2 + O_2 \rightarrow O_3 + O_2$	$6 \times 10^{-46} \times (1.3^{-2.8})$
2	$O + O_2 + N_2 \rightarrow O_3 + N_2$	$5.6 \times 10^{-46} \times (1.3^{-2.8})$
3	$O + O_3 \rightarrow O_2 + O_2$	$8 \times 10^{-18} \times \exp(-2060/4)$
4	$O + NO_2 \rightarrow NO + O_2$	$5.6 \times 10^{-7} \times \exp(180/40)$
5	$O + N\ O_3 \rightarrow O_2 + NO_2$	1.7×10^{-17}
6	$O + N_2O_5 \rightarrow NO_2 + NO_2 + O_2$	1×10^{-22}
7	$N + O_2 \rightarrow NO + O$	$1.5 \times 10^{-7} \times \exp(8)$
8	$N + O_3 \rightarrow NO + O_2$	1×10^{-22}
9	$N + NO \rightarrow N_2 + O$	$2.1 \times 10^{-11} \times \exp(0.25)$
10	$NO + O_3 \rightarrow NO_2 + O_2$	$3 \times 10^{-18} \times \exp(-3.8)$
11	$N + NO_2 \rightarrow N_2O + O$	$5.8 \times 10^{-18} \times \exp(0.55)$
12	$NO_2 + O_3 \rightarrow NO_3 + O_2$	$1.4 \times 10^{-19} \times \exp(-6.2)$
13	$O_2b1s + O_2 \rightarrow O_3 + O$	4.8×10^{-21}
14	$N_2 + O_2 \rightarrow N_2O + O$	$6 \times 10^{-20} \times (1.3^{0.55})$
15	$O^- + O \rightarrow O_2 + e$	$2 \times 10^{-16} \times (400^{0.5})$
16	$O^- + O_2 \rightarrow O_3 + e$	$3 \times 10^{-16} \times (400^{0.5})$
17	$O^- + O_2 \rightarrow O + O_2 + e$	$6.9 \times 10^{-16} \times \times (400^{0.5})$
18	$O_2 + O_2 \rightarrow O_3 + O$	$2.95 \times 10^{-27} \times \times (400^{0.5})$
19	$O^- + O_3 \rightarrow O_2 + O_2 + e$	$3 \times 10^{-16} \times \times (400^{0.5})$
20	$O^- + O_3 \rightarrow O_2^- + O_2$	$1.02 \times 10^{-17} \times \times (400^{0.5})$
21	$O_2^- + O \rightarrow O_3 + e$	$1.5 \times 10^{-16} \times \times (400^{0.5})$
22	$O + O_3 \rightarrow O_2 + O + O$	1.2×10^{-16}
23	$O_2 \rightarrow O_2$	0.2
24	$O_2 \rightarrow O$	10^{-5}
25	$N^+ + O_2 \rightarrow N + O_2^+$	3×10^{-16}

ionization, electron attachment, elastic collisions, excitation, recombination, neutral component collisions, and ion conversion processes. The schematic structure of SDBD and its boundary conditions is shown in Fig. 1. Copper electrode dimensions are 0.05 mm ×5 mm, and the dielectric dimensions are 0.5 mm ×10 mm. We employ five boundary layers and a 1.4 stretching factor for the system's whole boundary while meshing this structure. A free triangular mesh with a maximum element size of 0.4 is employed for the entire geometry (Fig. 2).

Nitrogen, oxygen, and argon reactions with a mass fraction of 0.78, 0.21, and 0.01 are used to simulate air gas discharge. The electron impact reactions with active nitrogen species, such as nitrogen molecules N_2 and N_2^+, that are singly ionized are shown in Table 1. The interactions of electron impact with active oxygen species, such

Table 5: Atomic and molecule-to-molecule interactions with two and three bodies (Sohbatzadeh and Soltani, 2018).

Reactions	Formula	K^f ($m^3.s^{-1}.mol^{-1}$)
1	$N_2 + Ar + N_2^+ \rightarrow Ar + N_4^+$	1.8×10^6
2	$e + N_4^+ \rightarrow N_2 + N_2$	1.2×10^{11}
3	$O_2 + Ar + O_2^+ \rightarrow Ar + O_a^+$	2×10^5
4	$O_4^+ + Ar + O^- \rightarrow 2O_2 + Ar + O$	5.2×10^{11}
5	$Ar + O_4^+ \rightarrow Ar + O + O_2 + e + O^+$	6×10^7
6	$O^- + Ar + O_4^+ \rightarrow 2O_2 + O + Ar$	3.8×10^8
7	$N_2 + Ar + N_2^+ \rightarrow Ar + N_4^+$	1.8×10^6

Table 6: The interactions between electrons and Argon (Hagelaar, 2010; LXcat, 2023).

Reactions	Formula	Type	$\Delta\varepsilon$ (eV)
1	$e + Ar \rightarrow e + Ar$	Elastic	0
2	$e + Ar \rightarrow e + Ars$	Excitation	11.5
3	$e + Ars \rightarrow e + Ar$	Superelastic	-11.5
4	$e + Ar \rightarrow 2e + Ar^+$	Ionization	15.8
5	$e + Ars \rightarrow 2e + Ar^+$	Ionization	4.24
6	$Ars + Ars \rightarrow e + Ar + Ar^+$	Penning ionization	-
7	$Ars + Ar \rightarrow eAr + Ar$	Metastable quenching	-

as metastable oxygen O_2s, oxygen molecule O_2, and singly ionized oxygen molecule O_2^+, are shown in Table 2. Tables 3, 4, and 5 offer the two and three-body reaction rates between atoms and molecules. Table 6 shows all electron impact reactions with argon and its molecule-to-molecule reactions. Fifteen surface reactions are considered in addition to the aforementioned reactions, as indicated in Table 7.

3 Results and discussion

An SDBD plasma actuator's body force magnitude has been obtained from the simulations. The rate of species generation is significantly influenced by the dielectric substance. Dielectric materials are electrically insulating substances with low electrical conductivity. Numerous processes that alter the behavior of the plasma and the emergence of species may take place when it comes into contact with a dielectric substance (Fridman and Kennedy, 2016; Lieberman and Lichtenberg, 1994).

Table 7: Table of surface reactions in air discharge (Sohbatzadeh and Soltani, 2018).

Reactions	Formula	TSticking Coefficient
1	O_2a1d $\rightarrow O_2$	1
2	$O_2$45 $\rightarrow O_2$	1
3	O_2bls $\rightarrow O_2$	1
4	$O_2 \rightarrow O_2$	1
5	$O_2^+ \rightarrow O_2$	1
6	$O^+ \rightarrow O$	1
7	$O^- \rightarrow O$	1
8	O1s $\rightarrow$ O	1
9	O1d $\rightarrow$ O	1
10	$N^+ \rightarrow N$	1
11	Ars $\rightarrow$ Ar	1
12	$Ar^+ \rightarrow$ Ar	1
13	N_2s $\rightarrow N_2$	1
14	$N_2^+ \rightarrow N_2$	1

In this study, we investigated how four different dielectric materials affected plasma properties that change the magnitude of body force in the plasma actuator. Figure 3 displays the electrical potential when plasma is formed. The grounded electrode has zero potential, while the power electrode has a voltage of 1.5 kV with a Gaussian shape.

Electron density and temperature play a vital role in plasma and are the initiators of many plasma reactions. And in many applications, the effect of electron density has been investigated (Mehrabifard et al., 2023; Tanaka et al., 2015), and it is an effective factor for the plasma actuators. The evaluation of electron temperature at 6 ns for various dielectric materials is shown in Fig. 4. Moving away from the power electrode causes the electron temperature to decrease from its highest value. As the figure shows, the temperature changes for each dielectric material were almost in the same range. Changing materials does not make a significant difference in electron temperature. The temperature of the electron is directly influenced by the electric field due to the implementation of a constant potential function, resulting in minimal fluctuations in temperature.

Then, once more, Eqs. (12) and (13) say this: the magnitude of the body force is directly influenced by the particle density. When all other factors remain the same, Fig. 5 illustrates how much the electron density changes with respect to the dielectric material. Using mica as dielectric results in electrons in its maximum value; quartz and silica have almost the same amount, 8.61×10^{14} m^{-3} and 8.22×10^{14} m^{-3}, respectively, and PTFE has the lowest value of 2.39×10^{14} m^{-3}. Changes in electron density are influenced by many causes, including surface charge accumulation and the photoionization effect. Among these factors, the alteration of the dielectric coefficient is particularly significant in determining the changes in surface charge accumulation. Indeed, the density rises in proportion to the increase in the dielectric coefficient.

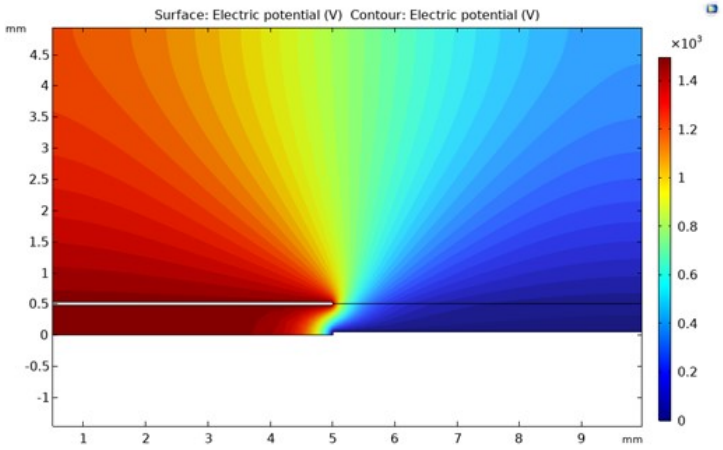

Figure 3: Distribution of electric potential for $V_{in} = 1.5$ kV.

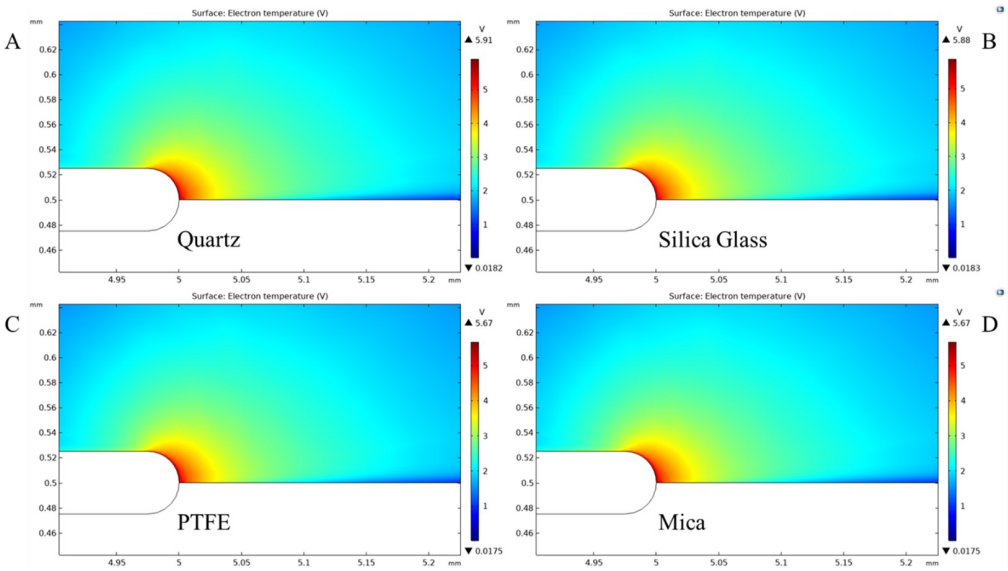

Figure 4: The electron temperature over 6 ns at 1.5 kV with Gaussian function for different dielectric materials (A) Quartz, (B) Silica Glass, (C) PTFE, (D) Mica.

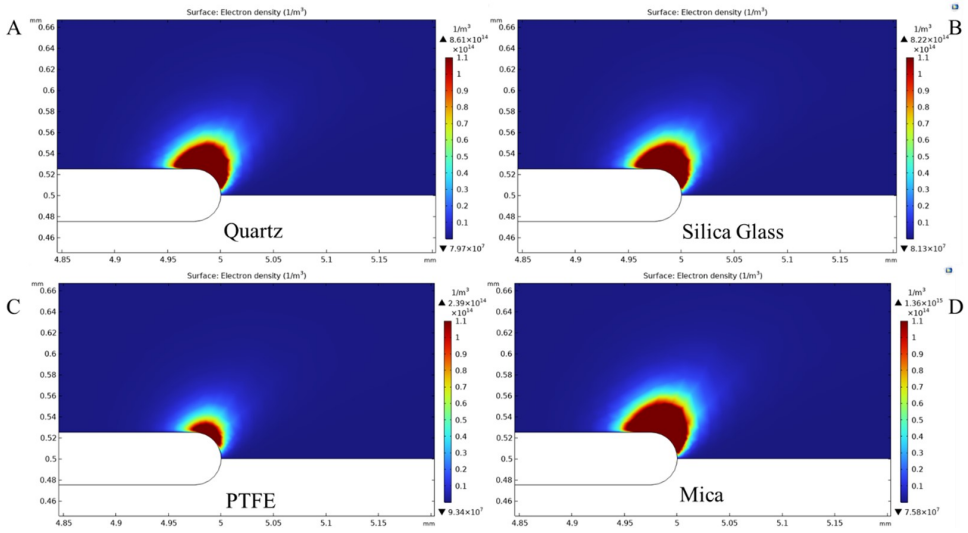

Figure 5: The electron densities over 6 ns at 1.5kV with Gaussian shape for different dielectric materials (A) Quartz, (B) Silica Glass, (C) PTFE, (D) Mica.

The ion densities are shown in Fig. 6. The n_{Ar^+}, $n_{N_2^+}$, $n_{O_2^+}$, $n_{N_4^+}$, n_{O_+}, $n_{O_{4+}}$, and n_{O_-} are the main species mea-

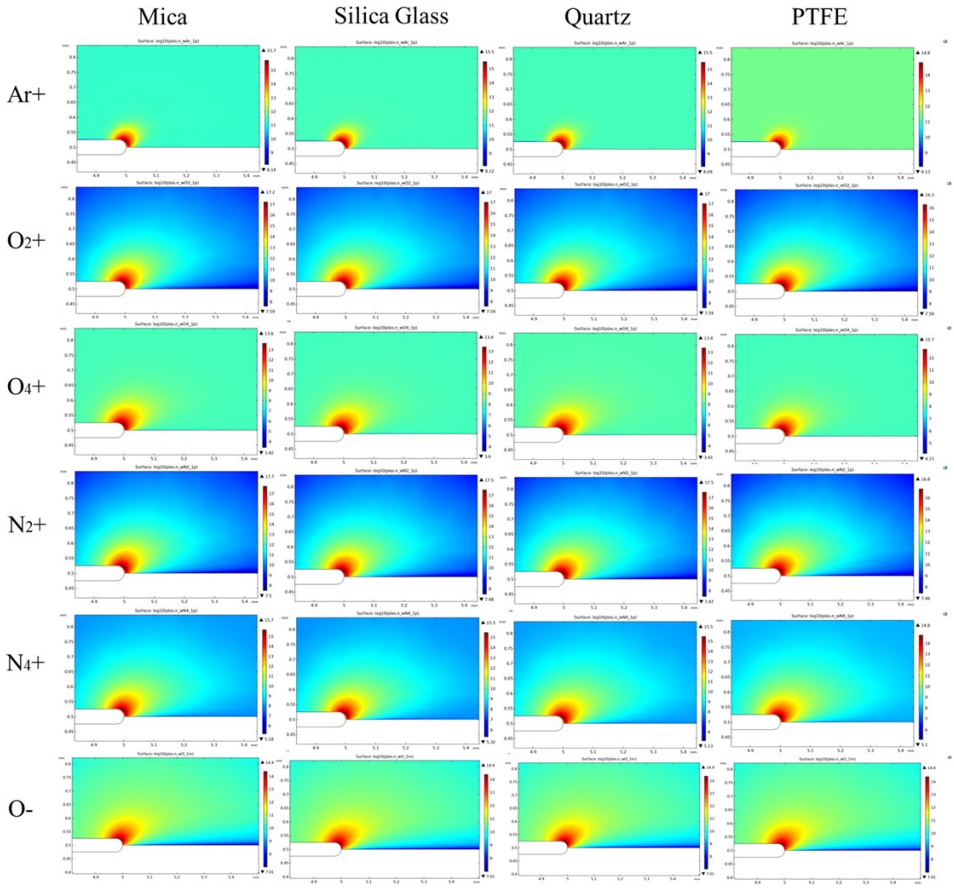

Figure 6: Two-dimensional distribution of the ion densities for different dielectric materials.

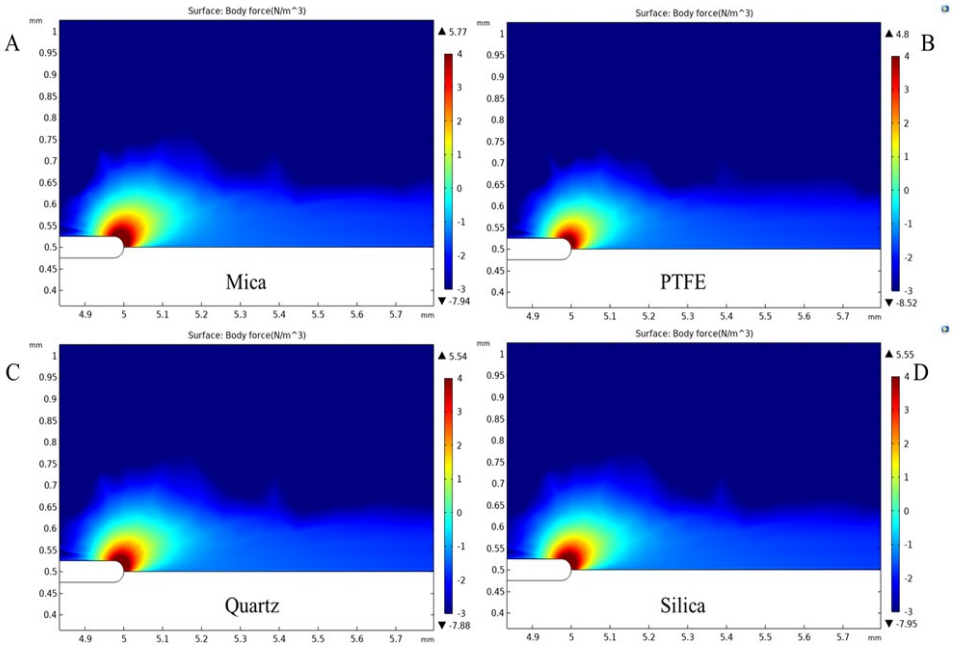

Figure 7: Magnitude of body force in the presence of different dielectric barrier discharge.

sured in this simulation in the presence of different dielectric materials. As Fig. 6 shows, all ion densities have a higher value in the presence of mica and the lowest for PTFE. And the value for quartz and silica glass shows almost the same ion density. As stated for the electron. The increase in surface charge accumulation will affect the density of ions, which is related to the dielectric coefficient.

The body force can be calculated from the difference between positive and negative charges and the magnitude of the normal field in the discharge space. According to

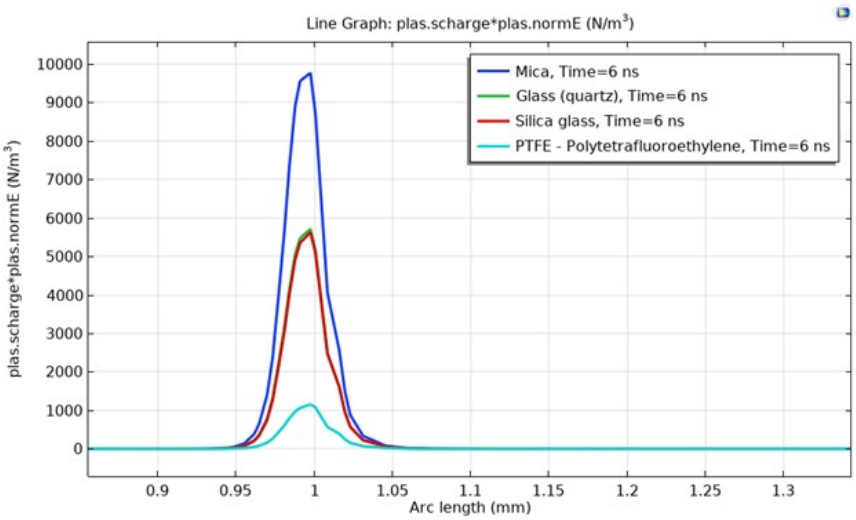

Figure 8: The body force is created on the surface of the electrode and the dielectric.

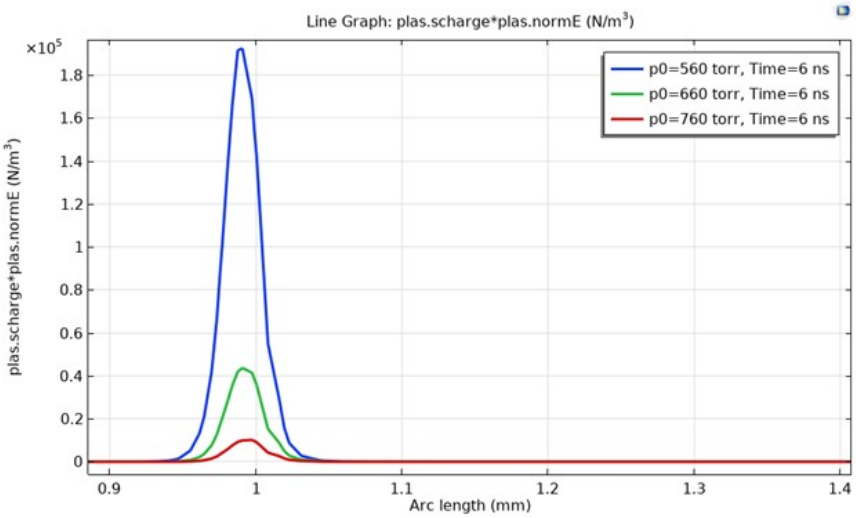

Figure 9: The effect of different pressures on body force.

Eq. (13), the logarithmic body force distribution for dielectric materials is shown in Fig. 7. To investigate more precisely, a hypothetical line on the surface of the electrode and dielectric is considered. This line's beginning and end points are $(x = 4, y = 0.54)$ and $(x = 8, y = 0.54)$. Figure 8 shows a non-logarithmic magnitude of the body force on this virtual line. As it is known, the force of the body is the highest for Mica, and its magnitude will be equal to 9800 N.m^{-3}. It will be equal to 5700 N.m^{-3}, 5600 N.m^{-3}, and 1100 N.m^{-3} for quartz, silica, and PTFE, respectively.

Gas pressure is one of the main parameters that can change the characteristics of the plasma; as a result, this causes a change in the magnitude of the body force in the plasma actuators. The pressure of 560, 660, and 760 torr are considered for plasma simulation. Figure 9 shows changes in body force magnitude for different pressures. The body force is measured on a virtual line on the upper part of the power electrode. As shown in the figure, the magnitude of body force changes dramatically by reducing pressure. The pressure was reduced by 100 torr in each stage, but significant changes were shown in body force.

Changing the dielectric coefficient, the electron energy distribution function changes around the power electrode, and this change leads to different ionization collisions around this electrode, which ultimately creates a difference in the ionization coefficient and volumetric force. As the ambient pressure changes, the ratio of the electric field to the ambient pressure will change, considering that the drift velocity is a function of the electric field-to-pressure ratio (E/P). On the other hand, this velocity is directly related to electron mobility; it can affect the changes in electron mobility. In fact, the set of these net charge density changes that lead to the production of propulsion force will be different.

4 Conclusions

Active current control is one of the areas where plasma is used. Additionally, modeling these systems before construction may save time and money and ensure the cre-

ation of an efficient system. From the outcome of our investigation, it is possible to conclude that without changing the main parameters and only by changing the type of dielectric material, the magnitude of the body force can be increased. Among the selected materials, using mica, we have the most body force. Furthermore, it is worth noting that pressure, being a crucial factor in plasma production, has shown that even the slightest alteration may lead to substantial variations in the body's force. Moreover, due to the significant change in body force, pressure is one of the parameters that should be considered in the actuator design. The simulation findings, performed with consideration of air gas discharge, can be valuable in the design of plasma drive systems for many applications, enabling the attainment of optimum outcomes via the selection of appropriate materials.

Conflict of Interest

The authors declare no potential conflict of interest regarding the publication of this work.

References

Abdelraouf, H., Elmekawy, A. M. N., and Kassab, S. Z. (2020). Simulations of flow separation control numerically using different plasma actuator models. *Alexandria Engineering Journal*, 59(5):3881–3896.

Abdollahzadeh, M., Páscoa, J., and Oliveira, P. (2012). Numerical modeling of boundary layer control using dielectric barrier discharge. In *MEFTE IV Conferencia Nacional em Mecanica de Fluidos*.

Assadi, I., Guesmi, A., Baaloudj, O., et al. (2022). Review on inactivation of airborne viruses using non-thermal plasma technologies: From MS2 to coronavirus. *Environmental Science and Pollution Research*, pages 1–13.

Benard, N. and Moreau, E. (2014). Electrical and mechanical characteristics of surface AC dielectric barrier discharge plasma actuators applied to airflow control. *Experiments in Fluids*, 55:1–43.

Boeuf, J.-P., Lagmich, Y., Unfer, T., et al. (2007). Electrohydrodynamic force in dielectric barrier discharge plasma actuators. *Journal of Physics D: Applied Physics*, 40(3):652.

Da Ponte, G., Sardella, E., Fanelli, F., et al. (2011). Atmospheric pressure plasma deposition of organic films of biomedical interest. *Surface and Coatings Technology*, 205:S525–S528.

Do, H., Kim, W., Mungal, M., et al. (2007). Bluff body flow separation control using surface dielectric barrier discharges. In *45th AIAA Aerospace Sciences Meeting and Exhibit*, page 939.

Fridman, A. and Kennedy, L. (2016). Nonequilibrium cold atmospheric pressure discharges. *Plasma Physics and Engineering*, pages 561–611.

Hagelaar, G. (2010). BOLSIG+ Electron Boltzmann equation solver. *Laboratoire Plasma et Conversion d'Energie (LAPLACE)*.

Hagelaar, G. and Pitchford, L. C. (2005). Solving the Boltzmann equation to obtain electron transport coefficients and rate coefficients for fluid models. *Plasma Sources Science and Technology*, 14(4):722.

Huang, J., Corke, T. C., and Thomas, F. O. (2006). Plasma actuators for separation control of low-pressure turbine blades. *AIAA Journal*, 44(1):51–57.

Jayaraman, B. and Shyy, W. (2008). Modeling of dielectric barrier discharge-induced fluid dynamics and heat transfer. *Progress in Aerospace Sciences*, 44(3):139–191.

Kazemi, M., Ghanooni, P., Mani, M., et al. (2021). Drag reduction of 3D bluff body using SDBD plasma actuators. *Proceedings of the Institution of Mechanical Engineers, Part D: Journal of Automobile Engineering*, 235(5):1461–1480.

Keidar, M. and Beilis, I. (2013). *Plasma engineering: applications from aerospace to bio and nanotechnology*. Academic Press.

Lieberman, M. A. and Lichtenberg, A. J. (1994). Principles of plasma discharges and materials processing. *MRS Bulletin*, 30(12):899–901.

Likhanskii, A., Shneider, M., Opaits, D., et al. (2007). Numerical modeling of DBD plasma actuators and the induced air flow. In *38th AIAA Plasmadynamics and Lasers Conference In conjunction with the 16th International Conference on MHD Energy Conversion*, page 4533.

Likhanskii, A. V., Shneider, M. N., Macheret, S. O., et al. (2008). Modeling of dielectric barrier discharge plasma actuator in air. *Journal of Applied Physics*, 103(5).

Little, J., Takashima, K., Nishihara, M., et al. (2010). High lift airfoil leading edge separation control with nanosecond pulse DBD plasma actuators. In *5th Flow Control Conference*, page 4256.

LXcat (2023). LXcat, University of Toulouse. *www.lxcat.net*.

Mahdavi, H. and Sohbatzadeh, F. (2019). The role of nonlinear body force in production of electric wind in an asymmetric surface dielectric barrier discharge. *Physica Scripta*, 94(8):085204.

Mehrabifard, R. (2023). Two-dimensional simulation of Argon dielectric barrier discharge (DBD) in plasma actuator structure with COMSOL Multiphysics. *arXiv preprint arXiv:2304.05698*.

Mehrabifard, R., Kabarkouhi, Z., Rezaei, F., et al. (2023). Physical understanding of the static magnetic field's synergistic enhancement of cold atmospheric pressure plasma treatment. *arXiv preprint arXiv:2304.05833*.

Mehrabifard, R., Mehdian, H., and Bakhshzadmahmoudi, M. (2017). Effect of non-thermal atmospheric pressure plasma on MDA-MB-231 breast cancer cells. *Pharmaceutical and Biomedical Research*, 3(3):12–16.

Mehrabifard, R., Mehdian, H., Hajisharifi, K., et al. (2020). Improving cold atmospheric pressure plasma efficacy on breast cancer cells control-ability and mortality using vitamin c and static magnetic field. *Plasma Chemistry and Plasma Processing*, 40:511–526.

Moreau, E. (2007). Airflow control by non-thermal plasma actuators. *Journal of physics D: applied physics*, 40(3):605.

Neretti, G., Cristofolini, A., and Borghi, C. A. (2014). Experimental investigation on a vectorized aerodynamic dielectric barrier discharge plasma actuator array. *Journal of Applied Physics*, 115(16).

Neretti, G., Cristofolini, A., Borghi, C. A., et al. (2012). Experimental results in DBD plasma actuators for air flow control. *IEEE Transactions on Plasma Science*, 40(6):1678–1687.

Omidi, J. and Mazaheri, K. (2020). Micro-plasma actuator mechanisms in interaction with fluid flow for wind energy applications: Physical parameters. *Physics of Fluids*, 32(7).

Pitchford, L. C., Alves, L. L., Bartschat, K., et al. (2017). Lxcat: An open-access, web-based platform for data needed for modeling low temperature plasmas. *Plasma Processes and Polymers*, 14(1-2):1600098.

Porter, C., McLaughlin, T., Enloe, C., et al. (2007). Boundary layer control using a DBD plasma actuator. In *45th AIAA Aerospace Sciences Meeting and Exhibit*, page 786.

Post, M. L. and Corke, T. C. (2006). Separation control using plasma actuators: Dynamic stall vortex control on oscillating airfoil. *AIAA Journal*, 44(12):3125–3135.

Sakiyama, Y., Graves, D. B., Chang, H.-W., et al. (2012). Plasma chemistry model of surface microdischarge in humid air and dynamics of reactive neutral species. *Journal of Physics D: Applied Physics*, 45(42):425201.

Sohbatzadeh, F. and Soltani, H. (2018). Time-dependent one-dimensional simulation of atmospheric dielectric barrier discharge in N2/O2/H2O using COMSOL Multiphysics. *Journal of Theoretical and Applied Physics*, 12:53–63.

Stafford, D. S. and Kushner, M. J. (2004). O-2 ((1) Delta) production in He/O-2 mixtures in flowing low pressure plasmas. *Journal of Applied Physics*, 96(5):2451–2465.

Szulga, N., Vermeersch, O., Forte, M., et al. (2015). Experimental and numerical study of boundary layer transition control over an airfoil using a DBD plasma actuator. *Procedia IUTAM*, 14:403–412.

Tanaka, H., Mizuno, M., Ishikawa, K., et al. (2015). Plasma with high electron density and plasma-activated medium for cancer treatment. *Clinical Plasma Medicine*, 3(2):72–76.

Tehrani, D. S., Abdizadeh, G., and Noori, S. (2022). Numerical modeling of dielectric barrier discharge actuators based on the properties of low-frequency plasmons. *Scientific Reports*, 12(1):10378.

Thomas, F. O., Kozlov, A., and Corke, T. C. (2008). Plasma actuators for cylinder flow control and noise reduction. *AIAA Journal*, 46(8):1921–1931.

Touchard, G. (2008). Plasma actuators for aeronautics applications-state of art review. *International Journal of Plasma Environmental Science and Technology*, 2(1):1–24.

Venezia, R. A., Orrico, M., Houston, E., et al. (2008). Lethal activity of nonthermal plasma sterilization against microorganisms. *Infection Control & Hospital Epidemiology*, 29(5):430–436.

Yu, H., Cui, X., Li, G., et al. (2023). Numerical investigation of flow separation control over rotor blades using plasma actuator. *AIAA Journal*, 61(3):1151–1167.

©2024 by the journal.

RPE is licensed under a Creative Commons Attribution-NonCommercial 4.0 International License (CC BY-NC 4.0).

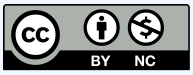

To cite this article:

Hajikhani, S., Mehrabifard, R., Soltani Ahmadi, H. (2024). A numerical analysis of the impact of gas pressure and dielectric material on the generation of body force in an air gas plasma actuator. *Radiation Physics and Engineering*, 5(2), 51-60.

DOI: 10.22034/rpe.2024.429773.1176

To link to this article: https://doi.org/10.22034/rpe.2024.429773.1176